

On the Computation of Square Roots and Inverse Square Roots of Gram Matrices for Surface Integral Equations in Electromagnetics

Rui Chen, *Member, IEEE*, Adrien Merlini, *Senior Member, IEEE*, and Francesco P. Andriulli, *Fellow, IEEE*

Abstract—Surface integral equations (SIEs)-based boundary element methods are widely used for analyzing electromagnetic scattering scenarios. However, after discretization of SIEs, the spectrum and eigenvectors of the boundary element matrices are not usually representative of the spectrum and eigenfunctions of the underlying surface integral operators, which can be problematic for methods that rely heavily on spectral properties. To address this issue, we delineate some efficient algorithms that allow for the computation of matrix square roots and inverse square roots of the Gram matrices corresponding to the discretization scheme, which can be used for revealing the spectrum of standard electromagnetic integral operators. The algorithms, which are based on properly chosen expansions of the square root and inverse square root functions, are quite effective when applied to several of the most relevant Gram matrices used for boundary element discretizations in electromagnetics. Tables containing different sets of expansion coefficients are provided along with comparative numerical experiments that evidence advantages and disadvantages of the different approaches. In addition, to demonstrate the spectrum-revealing properties of the proposed techniques, they are applied to the discretization of the problem of scattering by a sphere for which the analytic spectrum is known.

Index Terms—Boundary element method, fast algorithm, Gram matrix, surface integral equation.

I. INTRODUCTION

In the last few decades, the boundary element method (BEM) has been widely used for analyzing electromagnetic scattering from perfect electrically conducting (PEC) scatterers [1]–[3]. For such scatterers, BEM is typically applied to

This work has received support by the European Union – Next Generation EU within the PNRR project “Multiscale modeling and Engineering Applications” of the Italian National Center for HPC, Big Data and Quantum Computing (Spoke 6) – PNRR M4C2, Investimento 1.4 - Avviso n. 3138 del 16/12/2021 - CN00000013 National Centre for HPC, Big Data and Quantum Computing (HPC) - CUP E13C22000990001, from the European Research Council (ERC) under the European Union’s Horizon 2020 research and innovation programme (grant agreement No. 724846, project 321), from the National Natural Science Foundation of China (NSFC) under Grant 62201264 and Grant 62331016, from Foundation of Anhui Key Laboratory of Industrial Energy-Saving and Safety under Grant KFKT202306, and from the ANR Labex CominLabs under the project “CYCLE”. (*Corresponding author: Francesco P. Andriulli.*)

Rui Chen was with the Department of Electronics and Telecommunications, Politecnico di Torino, 10129 Turin, Italy. He is now with the School of Microelectronics (School of Integrated Circuits), Nanjing University of Science and Technology, Nanjing 210094, China and also with North Automatic Control Technology Institute, Taiyuan 030006, China (e-mail: rui.chen@njust.edu.cn).

Adrien Merlini is with the Microwave Department, IMT Atlantique, 29238 Brest, France (e-mail: adrien.merlini@imt-atlantique.fr).

Francesco P. Andriulli is with the Department of Electronics and Telecommunications, Politecnico di Torino, 10129 Turin, Italy (e-mail: francesco.andriulli@polito.it).

surface integral equations (SIEs), e.g., electric field integral equation (EFIE), magnetic field integral equation, and their linear combinations. In contrast to differential equation-based methods, BEM does not require the use of artificial absorbing boundary conditions for truncating the infinite domain and only requires the discretization of the scatterer’s surface with boundary elements, thus resulting in a comparatively lower number of unknowns [3].

To numerically solve SIEs, surface integral operators are first discretized by expanding the current on the scatterer’s surface with basis functions (the boundary elements), then testing functions are selected to test the resulting equation resulting in a fully discretized matrix equation system. Finally, direct solvers or iterative solvers coupled with fast matrix-vector product algorithms are used to solve these systems for the unknown current expansion coefficients [3].

For the above-described discretization of SIEs, however, the spectrum and eigenvectors of the boundary element matrices are not usually representative of the spectrum and eigenfunctions of the underlying surface integral operators. This is in part due to the fact that, in general, boundary elements do not form an orthonormal basis of the spaces they span and the operatorial eigenvalues could only be obtained by solving a generalized eigenvalue problem [4]. While this is not necessarily problematic for standard solution strategies, some numerical methods rely on delicate spectral manipulations that necessitate correspondence between the spectra of the operator to be discretized and the corresponding boundary element matrix [5]. To address this issue, one could use orthonormal basis functions, but they are often impractical. Other approaches are instead based on a *a posteriori* orthonormalization of the bases used in the discretization of the integral operators using square roots and inverse square roots of Gram matrices (see [5] and references therein). Several algorithms have been presented to compute these matrices (e.g. [6], [7]) and their theory is well-established. Nonetheless, the application of these schemes to the variety of Gram matrices appearing in the integral equations relevant scenarios is far from trivial as a specific set of approaches among many must be selected and the associated parameters need to be optimized to ensure a computational complexity compatible with traditional fast solution and iterative eigenproblem methods [8].

In this work, approaches for obtaining square roots and inverse square roots of several of the most relevant Gram matrices are delineated and tailored to all cases of interest. Moreover, the thorough performance analysis is presented

together with a comprehensive set of implementation oriented strategies. To numerically compute the square roots and inverse square roots of the Gram matrices, suitably chosen expansions of the square root and inverse square root scalar functions are used in combination with the theory of matrix functions [9]. Several algorithmic approaches for the evaluation of the square roots and inverse square roots of the Gram matrices are considered and tables containing expansion coefficients are provided. Numerical experiments illustrate the merits of the different approaches. Finally, to demonstrate the applicability of the techniques, numerical examples showing how the spherical harmonics spectrum of the EFIE operator can be recovered from a standard EFIE system matrix are presented. While most of the discussion focuses on the EFIE and related discretization schemes, the proposed methods are applicable to most of the standard electromagnetic and acoustic integral equations.

II. BACKGROUND

Let S denote the surface of a PEC scatterer residing in an unbounded homogeneous background medium. The permittivity and permeability of the background medium are ε and μ , respectively. The PEC scatterer is excited by an electromagnetic wave with the incident electric field $\mathbf{E}^{\text{inc}}(\mathbf{r})$. Upon excitation, the surface current $\mathbf{J}(\mathbf{r})$ is induced on S that generates the scattered electric field $\mathbf{E}^{\text{sca}}(\mathbf{r})$ in the background medium; $\mathbf{E}^{\text{sca}}(\mathbf{r})$ can be expressed as a function of $\mathbf{J}(\mathbf{r})$ as

$$\begin{aligned} \mathbf{E}^{\text{sca}}(\mathbf{r}) = -\mathcal{L}[\mathbf{J}](\mathbf{r}) = & -j\omega\mu \int_S g(\mathbf{r}, \mathbf{r}') \mathbf{J}(\mathbf{r}') ds' \\ & - \frac{j}{\omega\varepsilon} \nabla \int_S g(\mathbf{r}, \mathbf{r}') \nabla'_s \cdot \mathbf{J}(\mathbf{r}') ds'. \end{aligned} \quad (1)$$

Here, $g(\mathbf{r}, \mathbf{r}') = e^{-jkR}/(4\pi R)$ is the Green function, $k = \omega\sqrt{\mu\varepsilon}$ is the wavenumber, and $R = |\mathbf{r} - \mathbf{r}'|$ represents the distance between the field and source points. Note that, the time-harmonic factor $e^{j\omega t}$ is assumed and suppressed throughout this work.

The total electric field $\mathbf{E}^{\text{tot}}(\mathbf{r}) = \mathbf{E}^{\text{inc}}(\mathbf{r}) + \mathbf{E}^{\text{sca}}(\mathbf{r})$ satisfies the boundary condition $\hat{\mathbf{n}}(\mathbf{r}) \times \mathbf{E}^{\text{tot}}(\mathbf{r}) = 0$ at $\mathbf{r} \in S$, where $\hat{\mathbf{n}}(\mathbf{r})$ is the outward pointing unit normal vector. Inserting (1) into the above boundary condition yields EFIE as

$$\mathcal{T}[\mathbf{J}](\mathbf{r}) = -\hat{\mathbf{n}}(\mathbf{r}) \times \mathcal{L}[\mathbf{J}](\mathbf{r}) = -\hat{\mathbf{n}}(\mathbf{r}) \times \mathbf{E}^{\text{inc}}(\mathbf{r}). \quad (2)$$

To numerically solve (2) for $\mathbf{J}(\mathbf{r})$, S is discretized into a mesh using triangular patches. Then, $\mathbf{J}(\mathbf{r})$ is expanded using Rao-Wilton-Glisson (RWG) basis functions [10] as

$$\mathbf{J}(\mathbf{r}) = \sum_{n=1}^{N_E} \{\mathbf{j}\}_n \mathbf{f}_n(\mathbf{r}). \quad (3)$$

Here, N_E denotes the number of edges of the mesh, \mathbf{j} with dimension $N_E \times 1$ is the vector containing the unknown current expansion coefficients to be solved for, and the n^{th} RWG basis function $\mathbf{f}_n(\mathbf{r})$ is defined as

$$\mathbf{f}_n(\mathbf{r}) = \begin{cases} \frac{\mathbf{r} - \mathbf{r}_n^+}{2A_n^+}, & \text{if } \mathbf{r} \in t_n^+ \\ \frac{\mathbf{r}_n^- - \mathbf{r}}{2A_n^-}, & \text{if } \mathbf{r} \in t_n^- \end{cases}, \quad (4)$$

where t_n^+ and t_n^- are two triangular patches sharing the n^{th} edge, \mathbf{r}_n^+ and \mathbf{r}_n^- are the vertices of t_n^+ and t_n^- that do not belong to the n^{th} edge, and A_n^+ and A_n^- are the areas of t_n^+ and t_n^- , respectively.

Next, the rotated RWG functions $\hat{\mathbf{n}}(\mathbf{r}) \times \mathbf{f}_m(\mathbf{r})$, $m = 1, 2, \dots, N_E$, are used to test (2), resulting in the discretized EFIE matrix equation system

$$\mathbf{T}\mathbf{j} = \mathbf{v}. \quad (5)$$

Here, the entries of the boundary element matrix \mathbf{T} with dimension $N_E \times N_E$ and the right-hand side vector \mathbf{v} with dimension $N_E \times 1$ are

$$\{\mathbf{T}\}_{mn} = \langle \hat{\mathbf{n}}(\mathbf{r}) \times \mathbf{f}_m(\mathbf{r}), \mathcal{T}[\mathbf{f}_n](\mathbf{r}) \rangle \quad (6)$$

$$\{\mathbf{v}\}_m = -\langle \hat{\mathbf{n}}(\mathbf{r}) \times \mathbf{f}_m(\mathbf{r}), \hat{\mathbf{n}}(\mathbf{r}) \times \mathbf{E}^{\text{inc}}(\mathbf{r}) \rangle, \quad (7)$$

where $\langle \mathbf{a}(\mathbf{r}), \mathbf{b}(\mathbf{r}) \rangle = \int_{S_a} \mathbf{a}(\mathbf{r}) \cdot \mathbf{b}(\mathbf{r}) ds$ for vector functions, $\langle a(\mathbf{r}), b(\mathbf{r}) \rangle = \int_{S_a} a(\mathbf{r}) b(\mathbf{r}) ds$ for scalar functions and S_a is the support of $\mathbf{a}(\mathbf{r})$ or $a(\mathbf{r})$.

For certain applications, such as preconditioning [11], the electric field integral operator (EFIO) \mathcal{T} must also be discretized using Buffa-Christiansen (BC) basis functions $\mathbf{g}_n(\mathbf{r})$, $n = 1, 2, \dots, N_E$ [12]. The BC basis functions are dual functions with respect to the RWG basis functions and are defined on barycentrically refined triangular patches. The explicit definition of the BC basis function $\mathbf{g}_n(\mathbf{r})$ is omitted here and can be found in [12].

We denote the Gram matrices associated with the RWG and BC functions as $\mathbf{G}_{\mathbf{f},\mathbf{f}}$ and $\mathbf{G}_{\mathbf{g},\mathbf{g}}$. Their entries are $\{\mathbf{G}_{\mathbf{f},\mathbf{f}}\}_{mn} = \langle \mathbf{f}_m(\mathbf{r}), \mathbf{f}_n(\mathbf{r}) \rangle$ and $\{\mathbf{G}_{\mathbf{g},\mathbf{g}}\}_{mn} = \langle \mathbf{g}_m(\mathbf{r}), \mathbf{g}_n(\mathbf{r}) \rangle$, respectively.

Besides the above mentioned vector basis functions, i.e., the RWG and BC basis functions, used for the discretization of EFIE, scalar basis functions can also be used for the discretization of other SIEs, e.g., potential integral equations in electromagnetics [13]–[15] and standard integral equations in acoustics [16], [17].

In this work, two commonly used scalar basis functions, i.e., pyramid basis functions $\lambda_n(\mathbf{r})$, $n = 1, 2, \dots, N_V$ and the dual functions of the pyramid basis functions $\tilde{\lambda}_n(\mathbf{r})$, $n = 1, 2, \dots, N_P$, are considered, where N_V and N_P denote the number of vertices and triangular patches of the mesh, respectively. The dual pyramid basis functions $\tilde{\lambda}_n(\mathbf{r})$ are defined on the barycentrically refined triangular patches. The n^{th} pyramid basis function $\lambda_n(\mathbf{r})$ is defined to be equal to 1 at the n^{th} vertex, 0 at the other vertices, and linear on the triangular patches sharing the n^{th} vertex [18]. The explicit definition of the dual pyramid basis function $\tilde{\lambda}_n(\mathbf{r})$ is omitted here that can be found in [12]. Similarly, the Gram matrices associated with the pyramid and dual pyramid functions are $\mathbf{G}_{\lambda,\lambda}$ with dimension $N_V \times N_V$ and $\mathbf{G}_{\tilde{\lambda},\tilde{\lambda}}$ with dimension $N_P \times N_P$, whose entries are $\{\mathbf{G}_{\lambda,\lambda}\}_{mn} = \langle \lambda_m(\mathbf{r}), \lambda_n(\mathbf{r}) \rangle$ and $\{\mathbf{G}_{\tilde{\lambda},\tilde{\lambda}}\}_{mn} = \langle \tilde{\lambda}_m(\mathbf{r}), \tilde{\lambda}_n(\mathbf{r}) \rangle$, respectively.

The Gram matrices introduced above ($\mathbf{G}_{\mathbf{f},\mathbf{f}}$, $\mathbf{G}_{\mathbf{g},\mathbf{g}}$, $\mathbf{G}_{\lambda,\lambda}$, and $\mathbf{G}_{\tilde{\lambda},\tilde{\lambda}}$) are symmetric positive definite (SPD) and can be used for the normalizations of the EFIE boundary element matrix \mathbf{T} , the loop-to-RWG transformation matrix $\mathbf{\Lambda}$, and the star-to-RWG transformation matrix $\mathbf{\Sigma}$, where the explicit definitions of $\mathbf{\Lambda}$ and $\mathbf{\Sigma}$ can be found in [19]. As mentioned

in [5], using the normalized matrices $\tilde{\mathbf{T}}$, $\tilde{\mathbf{\Lambda}}$, and $\tilde{\mathbf{\Sigma}}$ instead of their standard counterparts \mathbf{T} , $\mathbf{\Lambda}$, and $\mathbf{\Sigma}$ allows for more efficient spectral manipulations for problems involving non-uniformly discretized geometries. The normalized matrices are obtained by multiplying the standard matrices with the inverse square roots of the corresponding Gram matrices, e.g., $\tilde{\mathbf{T}} = \sqrt{\mathbf{G}_{f,f}}^{-1} \mathbf{T} \sqrt{\mathbf{G}_{f,f}}^{-1}$. In Section III, the strategies of the computation of these square roots and inverse square roots of the Gram matrices are presented.

III. COMPUTATION OF THE SQUARE ROOTS AND INVERSE SQUARE ROOTS OF THE GRAM MATRICES

In the following, we will assume to deal with the SPD matrices. In this case, to compute the square roots and inverse square roots of the Gram matrices, a simple-to-define but expensive-to-compute approach is to leverage the singular value decomposition (SVD). The SVD of a real SPD matrix \mathbf{G} of dimension $N \times N$ is defined as

$$\mathbf{G} = \mathbf{U}\mathbf{S}\mathbf{U}^T, \quad (8)$$

where \mathbf{S} is a diagonal matrix of which the elements are the N singular values of \mathbf{G} , \mathbf{U} is a unitary matrix, and $\mathbf{G} = \{\mathbf{G}_{f,f}, \mathbf{G}_{g,g}, \mathbf{G}_{\lambda,\lambda}, \mathbf{G}_{\tilde{\lambda},\tilde{\lambda}}\}$. Given that the matrices under consideration are also invertible, their square root and inverse square root can be obtained as

$$\sqrt{\mathbf{G}} = \mathbf{U}\bar{\mathbf{S}}\mathbf{U}^T \quad (9)$$

$$\sqrt{\mathbf{G}}^{-1} = \mathbf{U}\bar{\mathbf{S}}^{-1}\mathbf{U}^T, \quad (10)$$

where $\bar{\mathbf{S}}$ is a diagonal matrix of which the diagonal entries are the square roots of that of \mathbf{S} . However, because of the computational cost of the SVD algorithm, this method quickly becomes unpractical for large problems. Note that, since the matrices under consideration are SPD, their respective square roots are unique [20].

In the following, the square roots and inverse square roots of the Gram matrices are expressed as

$$\sqrt{\mathbf{G}} = \sqrt{\|\mathbf{G}\|_2} \sqrt{\mathbf{G}/\|\mathbf{G}\|_2}, \quad (11)$$

$$\sqrt{\mathbf{G}}^{-1} = \sqrt{\|\mathbf{G}\|_2}^{-1} \sqrt{\mathbf{G}/\|\mathbf{G}\|_2}^{-1}, \quad (12)$$

where $\|\mathbf{G}\|_2$ denotes the L_2 -norm of \mathbf{G} , which can be computed using power methods. Then, because the Gram matrices under consideration are sparse, $\sqrt{\mathbf{G}/\|\mathbf{G}\|_2}$ and $\sqrt{\mathbf{G}/\|\mathbf{G}\|_2}^{-1}$ are numerically approximated using polynomial expansions based on the theory of matrix functions [9]. Finally, $\sqrt{\mathbf{G}}$ and $\sqrt{\mathbf{G}}^{-1}$ are computed by multiplying $\sqrt{\|\mathbf{G}\|_2}$ and $\sqrt{\|\mathbf{G}\|_2}^{-1}$ with the numerical approximations of $\sqrt{\mathbf{G}/\|\mathbf{G}\|_2}$ and $\sqrt{\mathbf{G}/\|\mathbf{G}\|_2}^{-1}$, respectively.

To further condense the treatments, we denote a matrix function by a single symbol f that corresponds to the matrix function either $\mathbf{X} \mapsto \sqrt{\mathbf{X}}$ or $\mathbf{X} \mapsto \sqrt{\mathbf{X}}^{-1}$ defined on the space of the SPD matrices of dimension $N \times N$. The numerical expression of $f(\mathbf{X})$ can be obtained by generalizing the numerical (polynomial or rational) approximation of its scalar function counterpart either $x \mapsto \sqrt{x}$ or $x \mapsto \sqrt{x}^{-1}$, $x \in \mathbb{R}^+$, respectively, to the matrix argument [9]. In the next

Section III-A, III-B, and III-C, three algorithmic approaches based on the polynomial approximations are presented to achieve this purpose.

A. Taylor Series Expansion

As the first algorithmic approach, the Taylor series expansion (TSE) [21] is used for the polynomial approximations of $x \mapsto \sqrt{x}$ and $x \mapsto \sqrt{x}^{-1}$. Using TSE, $x \mapsto \sqrt{x}$ and $x \mapsto \sqrt{x}^{-1}$ can be numerically expanded around $x = 1$ as

$$x \mapsto \begin{cases} \sqrt{x} \approx \sum_{n=0}^{N_T} c_n^{\text{TSE}} (x-1)^n \\ \sqrt{x}^{-1} \approx \sum_{n=0}^{N_T} \tilde{c}_n^{\text{TSE}} (x-1)^n \end{cases}. \quad (13)$$

Here, N_T is the TSE expansion order, and c_n^{TSE} and \tilde{c}_n^{TSE} are the n^{th} expansion coefficients of TSE for the approximations of \sqrt{x} and \sqrt{x}^{-1} , respectively, which can be computed as

$$c_n^{\text{TSE}} = \frac{\sqrt{x}^{(n)}|_{x=1}}{n!} \quad \text{and} \quad \tilde{c}_n^{\text{TSE}} = \frac{(1/\sqrt{x})^{(n)}|_{x=1}}{n!}. \quad (14)$$

The approximations of their matrix function counterparts $\mathbf{X} \mapsto \sqrt{\mathbf{X}}$ and $\mathbf{X} \mapsto \sqrt{\mathbf{X}}^{-1}$ are obtained by generalizing (13) to the matrix arguments as

$$\mathbf{X} \mapsto \begin{cases} \sqrt{\mathbf{X}} \approx \sum_{n=0}^{N_T} c_n^{\text{TSE}} (\mathbf{X} - \mathbf{I})^n \\ \sqrt{\mathbf{X}}^{-1} \approx \sum_{n=0}^{N_T} \tilde{c}_n^{\text{TSE}} (\mathbf{X} - \mathbf{I})^n \end{cases}. \quad (15)$$

Here, \mathbf{I} is the identity matrix with the same dimension as \mathbf{X} . The values of the first ten expansion coefficients of TSE $\{c_0^{\text{TSE}}, c_1^{\text{TSE}}, c_2^{\text{TSE}}, c_3^{\text{TSE}}, c_4^{\text{TSE}}, c_5^{\text{TSE}}, c_6^{\text{TSE}}, c_7^{\text{TSE}}, c_8^{\text{TSE}}, c_9^{\text{TSE}}\}$ and $\{\tilde{c}_0^{\text{TSE}}, \tilde{c}_1^{\text{TSE}}, \tilde{c}_2^{\text{TSE}}, \tilde{c}_3^{\text{TSE}}, \tilde{c}_4^{\text{TSE}}, \tilde{c}_5^{\text{TSE}}, \tilde{c}_6^{\text{TSE}}, \tilde{c}_7^{\text{TSE}}, \tilde{c}_8^{\text{TSE}}, \tilde{c}_9^{\text{TSE}}\}$ for the approximations of $\sqrt{\mathbf{X}}$ and $\sqrt{\mathbf{X}}^{-1}$ are $\{1, \frac{1}{2}, -\frac{1}{8}, \frac{1}{16}, -\frac{5}{128}, \frac{7}{256}, -\frac{21}{1024}, \frac{33}{2048}, -\frac{429}{32768}, \frac{715}{65536}\}$ and $\{1, -\frac{1}{2}, \frac{3}{8}, -\frac{5}{16}, \frac{35}{63}, -\frac{5}{256}, \frac{231}{1024}, -\frac{429}{2048}, \frac{32768}{32768}, -\frac{123155}{65536}\}$, respectively.

B. Chebyshev Polynomial Expansion

As the second algorithmic approach, the truncated Chebyshev polynomial series expansion (CPE) [22] is used for the polynomial approximations of the square root function and its reciprocal on the interval $x \in [n_0, 1]$ as

$$x \mapsto \begin{cases} \sqrt{x} \approx \sum_{n=0}^{N_C} {}'c_n^{\text{CPE}} T_n(x) \\ \sqrt{x}^{-1} \approx \sum_{n=0}^{N_C} {}'\tilde{c}_n^{\text{CPE}} T_n(x) \end{cases}. \quad (16)$$

Here, the primed summation indicates that the first term is halved, n_0 is a positive real number, N_C is the expansion order of CPE, and $T_n(x)$ is the shifted Chebyshev polynomial

of the first kind of order n defined on the interval $x \in [n_0, 1]$ as

$$T_n(x) = \begin{cases} 1 & \text{if } n = 0 \\ \frac{2x - (n_0 + 1)}{1 - n_0} & \text{if } n = 1 \\ 2 \left(\frac{2x - (n_0 + 1)}{1 - n_0} \right) T_{n-1}(x) - T_{n-2}(x) & \text{otherwise} \end{cases} \quad (17)$$

The Chebyshev series coefficients c_n^{CPE} and \tilde{c}_n^{CPE} for the approximations of \sqrt{x} and $\sqrt{x^{-1}}$ can be computed as [22]

$$c_n^{\text{CPE}} = \frac{2}{\pi} \int_{n_0}^1 \frac{\sqrt{x} T_n(x)}{\sqrt{-x^2 + (n_0 + 1)x - n_0}} dx \quad (18)$$

$$\tilde{c}_n^{\text{CPE}} = \frac{2}{\pi} \int_{n_0}^1 \frac{\sqrt{x^{-1}} T_n(x)}{\sqrt{-x^2 + (n_0 + 1)x - n_0}} dx, \quad (19)$$

which can be rewritten with special functions as

$$c_n^{\text{CPE}} = 2\sqrt{n_0} \frac{{}_3F_2 \left(\begin{matrix} -1/2 & 1/2 & 1 \\ 1-n & 1+n \end{matrix}; 1 - n_0^{-1} \right)}{\Gamma(1-n)\Gamma(1+n)} \quad (20)$$

$$\tilde{c}_n^{\text{CPE}} = \frac{2}{\sqrt{n_0}} \frac{{}_3F_2 \left(\begin{matrix} 1/2 & 1/2 & 1 \\ 1-n & 1+n \end{matrix}; 1 - n_0^{-1} \right)}{\Gamma(1-n)\Gamma(1+n)}, \quad (21)$$

where ${}_pF_q$ is the generalized hypergeometric function [23, eq. (16.2.1)] and Γ is the Euler gamma function.

Similarly, after the series expansions of $x \mapsto \sqrt{x}$ and $x \mapsto \sqrt{x^{-1}}$ in (16) are derived, their matrix function counterparts can be obtained by generalizing (16) to the matrix arguments as

$$\mathbf{X} \mapsto \begin{cases} \sqrt{\mathbf{X}} \approx \sum_{n=0}^{N_C} c_n^{\text{CPE}} T_n(\mathbf{X}) \\ \sqrt{\mathbf{X}^{-1}} \approx \sum_{n=0}^{N_C} \tilde{c}_n^{\text{CPE}} T_n(\mathbf{X}) \end{cases}, \quad (22)$$

where $T_n(\mathbf{X})$ is defined as

$$T_n(\mathbf{X}) = \begin{cases} \mathbf{I} & \text{if } n = 0 \\ \frac{2\mathbf{X} - (n_0 + 1)\mathbf{I}}{1 - n_0} & \text{if } n = 1 \\ \frac{2[2\mathbf{X} - (n_0 + 1)\mathbf{I}]}{1 - n_0} T_{n-1}(\mathbf{X}) - T_{n-2}(\mathbf{X}) & \text{otherwise} \end{cases} \quad (23)$$

Given (11) and (12), the spectrum of the SPD matrix to which CPE is applied lives in the interval $[n_0, 1]$, where n_0 is the inverse of the condition number of the matrix.

When using (22), the coefficients c_n^{CPE} and \tilde{c}_n^{CPE} must be computed for each matrix, since they are dependent on the condition number n_0^{-1} of the matrix argument. If this turns out to be inconvenient, tabulated values of coefficients can be used for the matrices that have a value of n_0 living in known ranges. Usage of such tabulated values will typically yield higher errors than the computation with the matrix-dependent coefficients and in Section IV we will provide numerical results for these two approaches designated respectively as

“CPE-1” for the matrix specific approach and “CPE-2” for the tabulated approach. For convenience, the values of c_n^{CPE} and \tilde{c}_n^{CPE} of CPE-2 are provided in Table I and Table II for given bounds on the Gram matrices conditioning (different n_0). The order N_C at which the Chebyshev series should be truncated to reach a target relative error δ on the matrix (defined in Section IV) has been obtained through numerical analyses and is reported in Table III. Note that, the direct evaluation of the sum in (22) is not necessarily optimal and other algorithms can be employed [24].

C. Padé Approximant Expansion

The last algorithmic approach we explore is the Padé approximant expansion (PAE) [25] for $x \mapsto \sqrt{x}$ and $x \mapsto \sqrt{x^{-1}}$ at $x = 1$ as

$$x \mapsto \begin{cases} \sqrt{x} \approx \frac{\sum_{n=0}^{N_A} c_n^{\text{PAE}} x^n}{\sum_{n=0}^{N_A} c_n^{\text{PAE}} x^{N_A-n}} \\ \sqrt{x^{-1}} \approx \frac{\sum_{n=0}^{N_A} c_n^{\text{PAE}} x^{N_A-n}}{\sum_{n=0}^{N_A} c_n^{\text{PAE}} x^n} \end{cases}. \quad (24)$$

Here, N_A is the expansion order of PAE, and c_n^{PAE} is the n^{th} expansion coefficient of PAE for the approximations of \sqrt{x} and $\sqrt{x^{-1}}$, which depends on N_A and can be obtained after solving the linear equation systems as presented in [26]. The numerical expressions of their matrix function counterparts are obtained by generalizing (24) to the matrix arguments as

$$\mathbf{X} \mapsto \begin{cases} \sqrt{\mathbf{X}} \approx \left(\sum_{n=0}^{N_A} c_n^{\text{PAE}} \mathbf{X}^{N_A-n} \right)^{-1} \left(\sum_{n=0}^{N_A} c_n^{\text{PAE}} \mathbf{X}^n \right) \\ \sqrt{\mathbf{X}^{-1}} \approx \left(\sum_{n=0}^{N_A} c_n^{\text{PAE}} \mathbf{X}^n \right)^{-1} \left(\sum_{n=0}^{N_A} c_n^{\text{PAE}} \mathbf{X}^{N_A-n} \right) \end{cases}. \quad (25)$$

The detailed values of the expansion coefficients c_n^{PAE} of PAE for $N_A = 0, 1, \dots, 9$ are provided in Table IV.

D. General Comments

Before the presentation of the numerical experiments, we would like to attract the reader’s attention on a few points. After the numerical expressions of $\sqrt{\mathbf{X}}$ and $\sqrt{\mathbf{X}^{-1}}$ in (15), (22), and (25) are obtained, the numerical expressions of $\sqrt{\mathbf{G}/\|\mathbf{G}\|_2}$ and $\sqrt{\mathbf{G}/\|\mathbf{G}\|_2}^{-1}$ are obtained with the substitution $\mathbf{X} = \mathbf{G}/\|\mathbf{G}\|_2$ in (15), (22), and (25) for TSE, CPE, and PAE, respectively. In addition, the normalization of \mathbf{G} (i.e., dividing \mathbf{G} by $\|\mathbf{G}\|_2$) in (11) and (12) is not a necessary step of our proposed algorithms. However, this normalization is often convenient for implementation and convergence purposes; when the matrices of interest are sparse, SPD, and well-conditioned, the power methods provide a very efficient way for computing $\|\mathbf{G}\|_2$.

IV. NUMERICAL RESULTS

In this section, several numerical experiments are presented to investigate the advantages and disadvantages of the proposed algorithmic approaches for the computation of $\sqrt{\mathbf{G}}$ and

$\sqrt{\mathbf{G}}^{-1}$, $\mathbf{G} \in \{\mathbf{G}_{f,f}, \mathbf{G}_{g,g}, \mathbf{G}_{\lambda,\lambda}, \mathbf{G}_{\tilde{\lambda},\tilde{\lambda}}\}$. To investigate the accuracy of the numerical approximations of the square roots and inverse square roots of the Gram matrices, the relative error δ is defined as

$$\delta = \frac{\|f^{\text{num}}(\mathbf{G}) - f^{\text{ref}}(\mathbf{G})\|_2}{\|f^{\text{ref}}(\mathbf{G})\|_2}. \quad (26)$$

Here, f denotes $\mathbf{G} \mapsto \sqrt{\mathbf{G}}$ or $\mathbf{G} \mapsto \sqrt{\mathbf{G}}^{-1}$, and the superscripts “num” and “ref” represent the numerical and reference values of $f(\mathbf{G})$ computed using the proposed algorithmic approaches in Section III and the computationally intensive method via SVD in (9) and (10), respectively.

For all the numerical experiments, a PEC sphere of radius 0.5 m, centered at the origin, and residing in free space is considered. The surface of the PEC sphere is non-uniformly discretized into three sets of meshes, denoted by “mesh-1”, “mesh-2”, and “mesh-3” with $\{N_E, N_P, N_V\} = \{1230, 820, 412\}$, $\{N_E, N_P, N_V\} = \{2193, 1462, 733\}$, and $\{N_E, N_P, N_V\} = \{4449, 2966, 1485\}$, respectively. The three sets of meshes have been selected so that the resulting Gram matrices are increasingly ill-conditioned for mesh-1, mesh-2, and mesh-3 with the condition numbers of $\{\mathbf{G}_{f,f}, \mathbf{G}_{g,g}, \mathbf{G}_{\lambda,\lambda}, \mathbf{G}_{\tilde{\lambda},\tilde{\lambda}}\}$ as $\{5.16, 5.74, 6.72, 9.11\}$, $\{20.45, 14.49, 29.12, 24.58\}$, and $\{615.61, 344.95, 361.91, 269.31\}$, respectively.

A. Accuracy of the Computation of the Square Roots and Inverse Square Roots of the Gram Matrices

As the first numerical experiment, the accuracy of the computation of $\sqrt{\mathbf{G}}$ and $\sqrt{\mathbf{G}}^{-1}$ using the proposed algorithms is investigated. Fig. 1(a)–(d) and Fig. 2(a)–(d) show the relative error of the computation of $\sqrt{\mathbf{G}_{f,f}}$, $\sqrt{\mathbf{G}_{g,g}}$, $\sqrt{\mathbf{G}_{\lambda,\lambda}}$, $\sqrt{\mathbf{G}_{\tilde{\lambda},\tilde{\lambda}}}$ and $\sqrt{\mathbf{G}_{f,f}}^{-1}$, $\sqrt{\mathbf{G}_{g,g}}^{-1}$, $\sqrt{\mathbf{G}_{\lambda,\lambda}}^{-1}$, $\sqrt{\mathbf{G}_{\tilde{\lambda},\tilde{\lambda}}}^{-1}$ for the three sets of meshes against the expansion order, respectively. As expected, the accuracy of the computation of $\sqrt{\mathbf{G}}$ and $\sqrt{\mathbf{G}}^{-1}$ using the proposed algorithms for all the sets of meshes increases with the increase of the expansion order. In addition, for a fixed expansion order and a given algorithm, the accuracy of the computation of $\sqrt{\mathbf{G}}$ and $\sqrt{\mathbf{G}}^{-1}$ for mesh-1 is higher than that for mesh-2 and mesh-3. This effect is a consequence of the lower condition numbers of the Gram matrices for mesh-1 than that for the other two sets of meshes. Moreover, for the low condition numbers (e.g., mesh-1), PAE converges faster than TSE and CPE. Fig. 1(a)–(d) and Fig. 2(a)–(d) also show that, for the same Gram matrix, the accuracy of the computation of $\sqrt{\mathbf{G}}^{-1}$ is generally lower than that of $\sqrt{\mathbf{G}}$ using the same expansion order for a given algorithm and a given set of meshes—in accordance with the report in Table III. In addition, the figures show that we could use CPE-2 as a good approximation of CPE-1 by directly using the bounds of the living known ranges of n_0 and their corresponding coefficients in Table I and Table II for CPE for convenience. The figures also show that the error behaviour of CPE-1 and CPE-2 converges towards one another when the actual value of n_0 for a given set of meshes and a given Gram matrix

corresponds to the value on n_0 used to select the CPE-2 tabulated coefficients.

B. Application to Spectral Analysis

As the second numerical experiment, the use of the proposed technique as a tool for the study and manipulation of the spectrum of the relevant integral operators is showcased for the problem of scattering by a PEC sphere of radius 1 m. The surface of the PEC sphere is uniformly discretized with $\{N_E, N_P, N_V\} = \{1080, 719, 361\}$ and the wavenumber is set to $k = 0.1 \text{ rad m}^{-1}$.

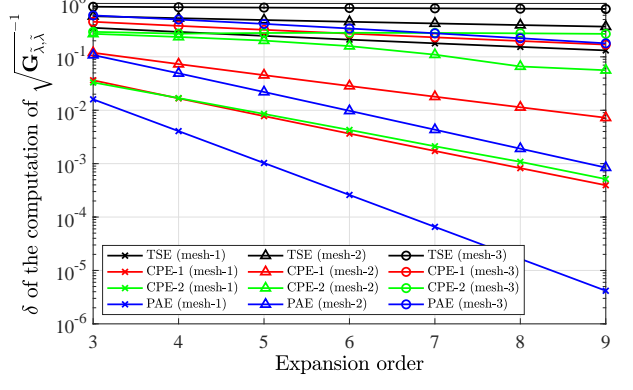
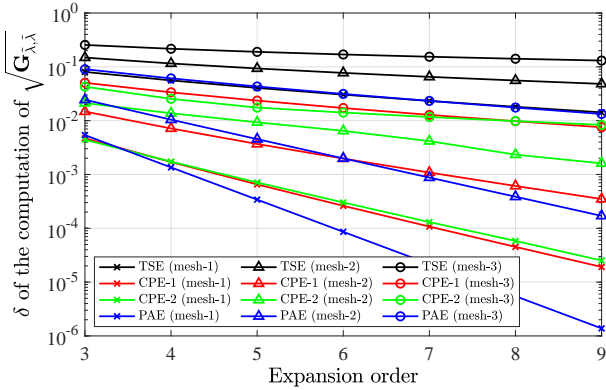
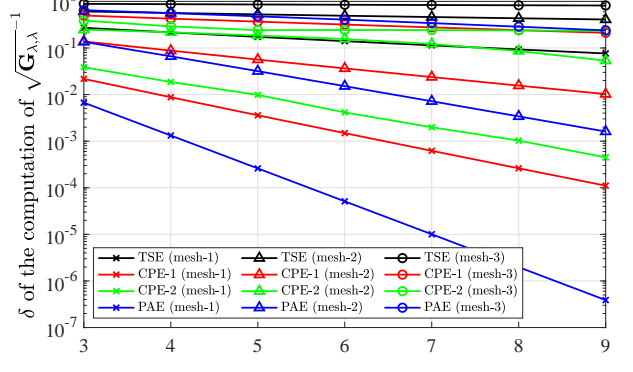
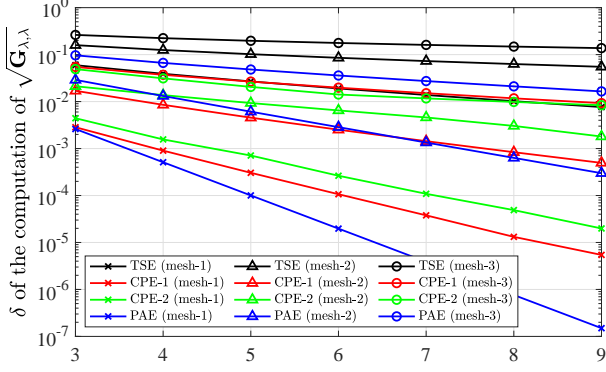
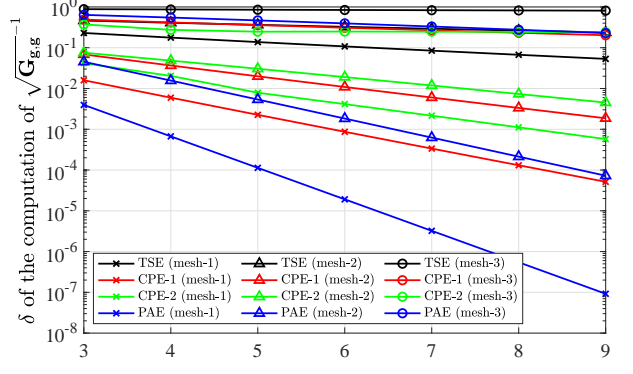
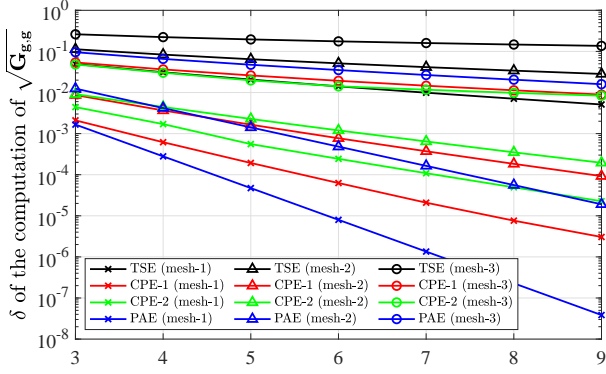
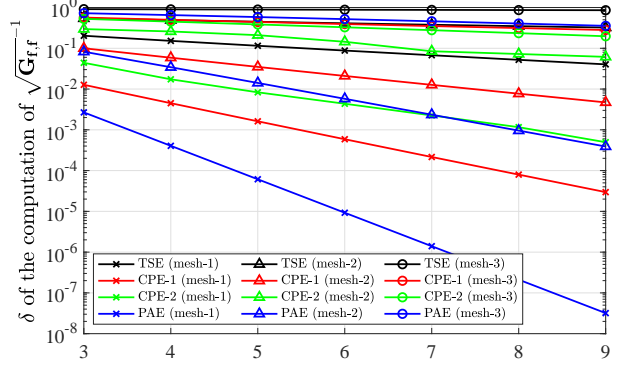
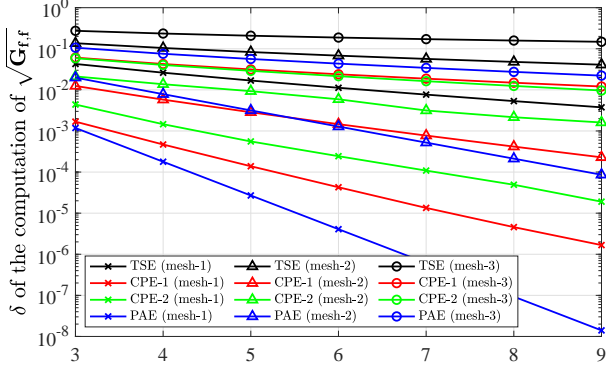
Fig. 3 compares both the singular values of the standard EFIE boundary element matrix \mathbf{T} and its normalized counterpart $\tilde{\mathbf{T}} = \sqrt{\mathbf{G}_{f,f}}^{-1} \mathbf{T} \sqrt{\mathbf{G}_{f,f}}$ with the analytic spectrum of \mathcal{T} obtained from a spherical harmonics analysis of the problem. The results are obtained with PAE for the numerical approximation of $\sqrt{\mathbf{G}_{f,f}}^{-1}$ with $N_A = 9$. As seen in Fig. 3, the singular values of the normalized matrix $\tilde{\mathbf{T}}$ show a good agreement with the analytic spectrum of \mathcal{T} while that of the standard matrix \mathbf{T} do not.

V. CONCLUSION

In this work, three algorithmic approaches are delineated for the computation of the square roots and reciprocal square roots of four relevant Gram matrices used for the zeroth-order discretization of the boundary element matrices in electromagnetics. General algorithms have been tailored to the specific integral equation scenario and tables containing the different sets of the expansion coefficients have been provided along with the comparative numerical experiments that evidence the advantages and disadvantages of the different strategies.

REFERENCES

- [1] A. F. Peterson, S. L. Ray, and R. Mittra, *Computational Methods for Electromagnetics*. New York, NY, USA: IEEE Press, 1998.
- [2] W. C. Gibson, *The Method of Moments in Electromagnetics*. 2nd ed. Boca Raton, FL, USA: CRC Press/Taylor Francis, 2014.
- [3] J.-M. Jin, *Theory and Computation of Electromagnetic Fields*. 2nd ed. New York, NY, USA: Wiley, 2015.
- [4] D. Boffi, “Compatible discretizations for eigenvalue problems,” in *Compatible Spatial Discretizations*, IMA Volumes in Mathematics and its Applications, vol. 142, pp. 121–142, Berlin: Springer, 2006.
- [5] A. Merlini, C. Henry, D. Consoli, L. Rahmouni, A. Dély and F. P. Andriulli, “Laplacian filtered loop-star decompositions and quasi-Helmholtz filters: Definitions, analysis, and efficient algorithms,” *IEEE Trans. Antennas Propag.*, vol. 71, no. 12, pp. 9289–9302, Dec. 2023.
- [6] E. D. Denman and A. N. Beavers, “The matrix sign function and computations in systems,” *Applied Mathematics and Computation*, vol. 2, no. 1, pp. 63–94, Jan. 1976.
- [7] N. J. Higham, “Newton’s method for the matrix square root,” *Mathematics of Computation*, vol. 46, no. 174, pp. 537–549, Apr. 1986.
- [8] G.W. Stewart, “A Krylov-Schur algorithm for large eigenproblems,” *SIAM J. Matrix Anal. Appl.*, vol. 23, issue 3, pp. 601–614, 2001.
- [9] N. J. Higham, *Functions of Matrices: Theory and Computation*. Philadelphia, PA, USA: SIAM, 2008.
- [10] S. Rao, D. Wilton, and A. Glisson, “Electromagnetic scattering by surfaces of arbitrary shape,” *IEEE Trans. Antennas Propag.*, vol. AP-30, no. 3, pp. 409–418, May 1982.
- [11] F. P. Andriulli, K. Cools, I. Bogaert and E. Michielssen, “On a well-conditioned electric field integral operator for multiply connected geometries,” *IEEE Trans. Antennas Propag.*, vol. 61, no. 4, pp. 2077–2087, Apr. 2013.
- [12] A. Buffa and S. Christiansen, “A dual finite element complex on the barycentric refinement,” *Math. Comput.*, vol. 76, pp. 1743–1769, 2007.



(d)

(d)

Fig. 1. Relative error of the computation of (a) $\sqrt{\mathbf{G}_{f,f}}^{-1}$, (b) $\sqrt{\mathbf{G}_{g,g}}^{-1}$, (c) $\sqrt{\mathbf{G}_{\lambda,\lambda}}^{-1}$, and (d) $\sqrt{\mathbf{G}_{\lambda,\lambda}}^{-1}$ using TSE, CPE-1, CPE-2, and PAE for mesh-1, mesh-2, and mesh-3 against the expansion order.

Fig. 2. Relative error of the computation of (a) $\sqrt{\mathbf{G}_{f,f}}^{-1}$, (b) $\sqrt{\mathbf{G}_{g,g}}^{-1}$, (c) $\sqrt{\mathbf{G}_{\lambda,\lambda}}^{-1}$, and (d) $\sqrt{\mathbf{G}_{\lambda,\lambda}}^{-1}$ using TSE, CPE-1, CPE-2, and PAE for mesh-1, mesh-2, and mesh-3 against the expansion order.

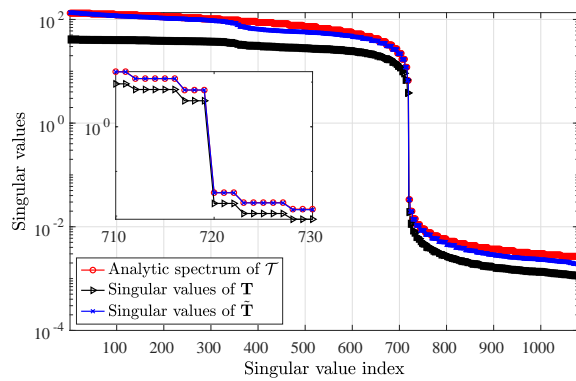


Fig. 3. Comparison of the singular values of \mathbf{T} and $\tilde{\mathbf{T}}$ with the associated analytic spectrum of \mathcal{T} including a zoom around singular value index 720.

- [13] W. C. Chew, "Vector potential electromagnetics with generalized gauge for inhomogeneous media: Formulation (invited paper)," *Prog. Electromagn. Res.*, vol. 149, pp. 69–84, 2014.
- [14] F. Vico, L. Greengard, M. Ferrando, and Z. Gimbutas, "The decoupled potential integral equation for time-harmonic electromagnetic scattering," *Commun. Pure Appl. Math.*, vol. 69, no. 4, pp. 771–812, Apr. 2016.
- [15] R. Chen, H. A. Ulku, F. P. Andriulli and H. Bagci, "On the low-frequency behavior of vector potential integral equations for perfect electrically conducting scatterers," *IEEE Trans. Antennas Propag.*, vol. 70, no. 12, pp. 12411–12416, Dec. 2022.
- [16] R. Chen, Y. Shi, S. B. Sayed, M. Lu, and H. Bagci, "On the spurious resonance modes of time domain integral equations for analyzing acoustic scattering from penetrable objects," *J. Acoust. Soc. Am.*, vol. 151, no. 2, pp. 1064–1076, Feb. 2022.
- [17] R. Chen, S. B. Sayed, N. Alharthi, D. Keyes, and H. Bagci, "An explicit marching-on-in-time scheme for solving the time domain Kirchhoff integral equation," *J. Acoust. Soc. Am.*, vol. 146, no. 3, pp. 2068–2079, Sep. 2019.
- [18] S. Y. Chen, W. C. Chew, J. M. Song, and J. -S. Zhao, "Analysis of low frequency scattering from penetrable scatterers," *IEEE Trans. Geosci. Remote Sens.*, vol. 39, no. 4, pp. 726–735, Apr. 2001.
- [19] S. B. Adrian, A. Dely, D. Consoli, A. Merlini, and F. P. Andriulli, "Electromagnetic integral equations: Insights in conditioning and preconditioning," *IEEE Open J. Antennas Propag.*, vol. 2, pp. 1143–1174, Oct. 2021.
- [20] C. R. Johnson, K. Okubo, and R. Reams, "Uniqueness of matrix square roots and an application," *Linear Algebra and its Applications*, vol. 323, no. 1–3, pp. 51–60, Jan. 2001.
- [21] B. Taylor, *Methodus Incrementorum Directa et Inversa*. London, UK: Impensis Gulielmi Innys, 1717.
- [22] J. C. Mason and C. D. Handscomb, *Chebyshev Polynomials*. London, UK: Chapman & Hall, 2002.
- [23] F. W. J. Olver, *NIST Handbook of Mathematical Functions*. Cambridge, UK: Cambridge University Press, 2010.
- [24] C. W. Clenshaw, "A note on the summation of Chebyshev series," *Mathematics of Computation*, vol. 9, no. 51, pp. 118–120, 1955.
- [25] G. A. Baker and P. Graves-Morris, *Padé Approximants*. Cambridge, UK: Cambridge University Press, 1996.
- [26] Y. Song, N. Sebe and W. Wang, "Fast differentiable matrix square root and inverse square root," *IEEE Trans. Pattern Anal. Mach. Intell.*, vol. 45, no. 6, pp. 7367–7380, Jun. 2023.